Article

Transport and Field Emission Properties of MoS$_2$ Bilayers

Francesca Urban [1,2], **Maurizio Passacantando** [3] (iD), **Filippo Giubileo** [2] (iD), **Laura Iemmo** [1,2] (iD)
and Antonio Di Bartolomeo [1,2,*] (iD)

[1]   Department of Physics "E.R. Caianiello", University of Salerno, 84084 Fisciano, Italy; furban@unisa.it (F.U.);
       liemmo@unisa.it (L.I.)
[2]   CNR-SPIN Salerno, 84084 Fisciano, Italy; filippo.giubileo@spin.cnr.it
[3]   Department of Physical and Chemical Sciences, University of L'Aquila, and CNR-SPIN L'Aquila,
       67100 L'Aquila, Italy; maurizio.passacantando@aquila.infn.it
*   Correspondence: adibartolomeo@unisa.it; Tel.: +39-089-969-189

Abstract: We report the electrical characterization and field emission properties of MoS$_2$ bilayers deposited on a SiO$_2$/Si substrate. Current–voltage characteristics are measured in the back-gate transistor configuration, with Ti contacts patterned by electron beam lithography. We confirm the n-type character of as-grown MoS$_2$ and we report normally-on field-effect transistors. Local characterization of field emission is performed inside a scanning electron microscope chamber with piezo-controlled tungsten tips working as the anode and the cathode. We demonstrate that an electric field of $\sim$ 200 V/µm is able to extract current from the flat part of MoS$_2$ bilayers, which can therefore be conveniently exploited for field emission applications even in low field enhancement configurations. We show that a Fowler–Nordheim model, modified to account for electron confinement in two-dimensional (2D) materials, fully describes the emission process.

Keywords: Transition metal dichalcogenides; MoS$_2$; field-effect transistor; field emission

1. Introduction

Over the past decade, graphene and graphene-like materials have attracted a lot of attention. Due to its two-dimensional (2D) nature and several extraordinary properties, such as high mobility and current carrying capability, chemical stability, and mechanical robustness, graphene in particular has been the most commonly chosen material for new electronic devices [1,2]. However, the absence of an intrinsic bandgap has hampered its application as a transistor channel [3,4] and has paved the way for the study of alternative 2D materials with semiconducting behavior, such as the transition metal dichalcogenides (TMDs) [5,6]. The TMD family, which comprises MX$_2$ compounds where M is a transition metal (Mo, W, etc.) and X a chalcogen (S, Se, Te), is gaining popularity in scientific and engineering research. In particular, molybdenum disulfide (MoS$_2$) is intensively studied for its ease of fabrication and direct bandgap suitable for optoelectronic applications [7–10].

Similarly to graphene, MoS$_2$ can be mechanically exfoliated from a bulk material and transferred onto a substrate [6]; however, single-crystal and large-scale flakes with a controlled number of layers are more easily produced by chemical vapor deposition (CVD) [11]. MoS$_2$ presents a structure consisting of a hexagonal plane of Mo atoms sandwiched between two planes of S atoms. Each layer is bonded to another one by van der Waals interactions to form the bulk structure. MoS$_2$ is considered a good candidate for electronic and optoelectronic applications because it offers control on the width of the energy bandgap through the number of layers [12], even though its mobility is typically only a few tens cm^{2}V^{-1}s^{-1} [8]. Indeed, multilayer MoS$_2$ shows an indirect bandgap of 1.2 eV which increases with the decreasing number of layers, becoming direct and of 1.8–1.9 eV for monolayers. The presence

of an energy gap enables MoS_2 transistors with a high on/off ratio ($> 10^7$) [13] and low subthreshold swing (below 70 mV/decade) [14]; moreover, a field effect mobility of about 200 $cm^2V^{-1}s^{-1}$ has been experimentally achieved [15]. Additional features such as high photoresponsivity [10,16] and spin–orbit splitting [17] have been investigated, opening the route for applicability of MoS_2 for optoelectronic and spintronic devices [10,18].

In this paper, we characterize the transport properties of bilayer MoS_2 field-effect transistors (FET) in the back-gate configuration. Furthermore, taking advantage of contacted MoS_2 flakes, we investigate their local field emission behavior. Compared with monolayers, bilayers are less affected by ambient exposure [19] and tend to form smaller Schottky barriers with metal contacts [20]; thus, they are more suitable for field emission applications.

Field emission (FE) is a quantum mechanical phenomenon in which electrons, extracted from a conductor or a semiconductor surface upon application of an intense electric field, flow in vacuum from a cathode to an anode. Classic field emission theory was developed by Fowler and Nordheim [21] for planar electrodes, but it is usually also applied to electrodes forming sharp tips [22]. Actually, tips with small radius of curvature enable enhancement of the local electric field, thereby requiring a reduced anode-to-cathode field for electron extraction [23]. Nanostructures, such as nanoparticles [24,25], nanowires [26], and nanotubes [23,27–30] or 2D materials [31,32], for their intrinsically sharp edges and high aspect ratio, are natural field emission sources. Indeed, semiconducting or metallic nanostructured materials have been considered for FE applications in vacuum electronics [33], flat panel displays [34], electron microscopy [35], X-ray tubes [36,37], etc.

To date, FE from MoS_2 has been very poorly characterized. There are few works concerning field emission measurements on MoS_2 nanostructures, like single- and multilayer flakes, nanoflowers, and films that are edge-terminated vertically aligned (ETVA) [38]. It has also been reported that ultra-thin ETVA-MoS_2 films present FE characteristics comparable to those of carbon-based structures [39–41].

Here, we measure FE current from the flat part of MoS_2 bilayers at a turn-on field of 230 V/µm. Despite the fact that we operate under no field enhancement condition, we find a local electric field magnified by a factor of 10 at the cathode–anode distance d = 75 nm and find that the field amplification factor increases linearly with d. Remarkably, we show that FE from MoS_2 bilayers follows a modified Fowler–Nordheim (FN) model recently proposed to include the effect of the confinement in 2D materials [42]. We highlight that, to the best of our knowledge, field emission from MoS_2 bilayers has not been reported before. Our study, demonstrating its suitability as a field emitter, aims to exploit MoS_2 in vacuum electronics, thus extending its use as an electrode in heterojunctions and channel in field-effect transistors.

2. Materials and Methods

The MoS_2 flakes were grown by CVD at 750 K (using S and MoO_3 as precursors) on p-doped Si substrate covered by 300 nm of SiO_2. The process yielded mainly bilayers and multilayers randomly distributed on the substrate. From scanning electron microscope (SEM, LEO 1530, Zeiss, Oberkochen, Germany) imaging, we often found traces of unreacted MoO_3 precursor on the flake, as shown in Figure 1a, which displays a typical back-gated field-effect transistor with Ti/Au metal leads. Such residuals can affect the carrier mobility. A schematic of the device, consisting of a TLM structure (Transfer Length Method) with back gate, is reported in Figure 1b.

We used the silicon substrate as a common back gate and metal leads, patterned by standard electron beam lithography and a lift-off process, as drain and source. The metal leads are made of Ti (20 nm) and Au (130 nm) deposited as contact and cover layers, respectively.

MoS_2 flakes were characterized by Raman spectroscopy before device fabrication in order to identify the number of layers. The Raman spectrum reported in Figure 1c shows two identifying peaks: A_{1g} associated with the out-of-plane vibration of sulfur atoms and E_{2g}^1 resulting from the in-plane vibrations of Mo and S atoms [43]. The two peaks are separated by 21 cm^{-1}, indicating bilayer flakes.

Micro-Raman spectroscopy mapping evidenced uniform thickness across the whole flakes; in few cases, we observed thinning in localized regions.
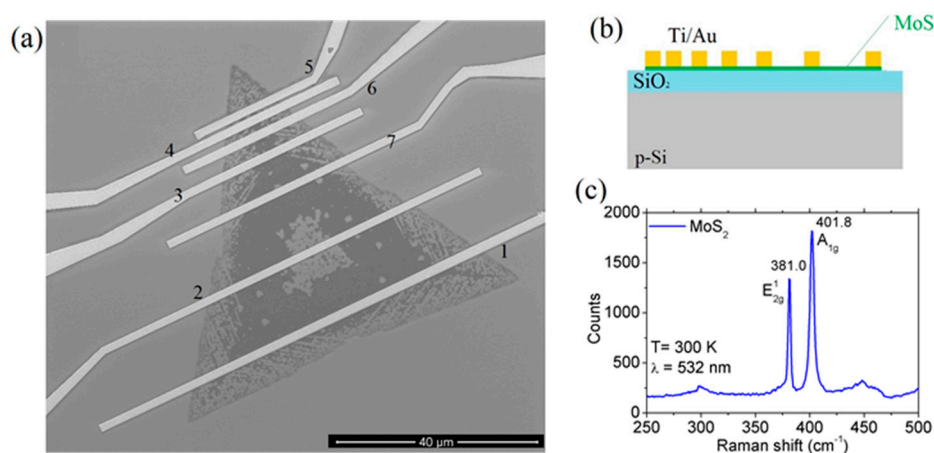
Figure 1. (**a**) SEM image of a Ti/Au contacted MoS_2 flake; (**b**) Schematic cross section of the field-effect device; (**c**) Raman spectrum of the flake.

In the following, the transistor characterization refers to contacts 4 (drain) and 5 (source), as marked in Figure 1a, i.e., to the device with the shortest channel, which is the most interesting from an application perspective. The distance between the two contacts, i.e., the channel length, is $L = 0.57\ \mu m$, while the channel width is $W \approx 11.4\ \mu m$.

Electrical measurements were performed using a Keithley 4200 SCS (source measurement unit, Tektronix, Beaverton, OR, USA) connected to a Janis ST-500 (Janis Research Company, ST-500, Woburn, MA, USA) probe station at room temperature and pressure of ~ 3 mbar.

Field emission measurements were carried out at a pressure $< 10^{-6}$ mbar in a SEM vacuum chamber endowed with two piezo-controlled tungsten tips (W-tips) with nanometric resolution.

Considering that the presence of impurities and precursor residues could alter the emission process from MoS_2, we chose emitting areas that were cleaner and more homogeneous. We did not observe significant differences in these zones and we report only one dataset in the following. We also tried field emission from regions covered by MoO_3, but we did not observe any signal. This is likely due to the 6.6 eV high work function of MoO_3 [44].

3. Results

3.1. Transistor Characterization

Figure 2 reports the electrical transport characterization of the back-gate MoS_2 transistor. The output characteristics $I_{ds} - V_{ds}$ (Figure 2a) were measured from -80 V to 10 V at gate voltage steps of 10 V. A channel resistance decrease, resulting in higher current, is observed for gate voltage, V_{gs}, varying from negative to positive voltages. This is further evidenced by the transfer $I_{ds} - V_{gs}$ characteristics, shown in Figure 2b for a given drain–source bias voltage ($V_{ds} = 0.5$ V).

The transfer curve discloses an n-type behavior with normally on channel at $V_{gs} = 0$ V. The off-state of the transistor is reached below the negative gate voltage of -80 V that we safely adopted as the lower limit for V_{gs} to prevent SiO_2 gate dielectric leakage or breakdown. The limited range of V_{gs} results in the apparent low on/off ratio of the transistor, which is essentially not turned off over the sweeping interval. Nevertheless, the measured portion of transfer curve is enough to estimate the threshold voltage. Given that $I_{ds} \propto (V_{gs} - V_{th})$, the threshold voltage corresponds to the x-axis intercept of the straight-line fitting of the current in linear scale and results in $V_{th} \approx -70$ V. We calculate the subthreshold swing as $SS = dV_{gs}/d(\log I_{ds}) = 20$ V/decade using the transfer blue

curve. The high value of SS, which is likely overestimated due to the fitting region being too close to V_{th}, is expected because of the low-efficiency back-gate configuration with thick gate oxide.

Remarkably, the prevailing on-state over a wide V_{gs} range and the n-type doping suggest that the MoS_2 flake can be suitable for electron extraction, i.e., for field emission applications.
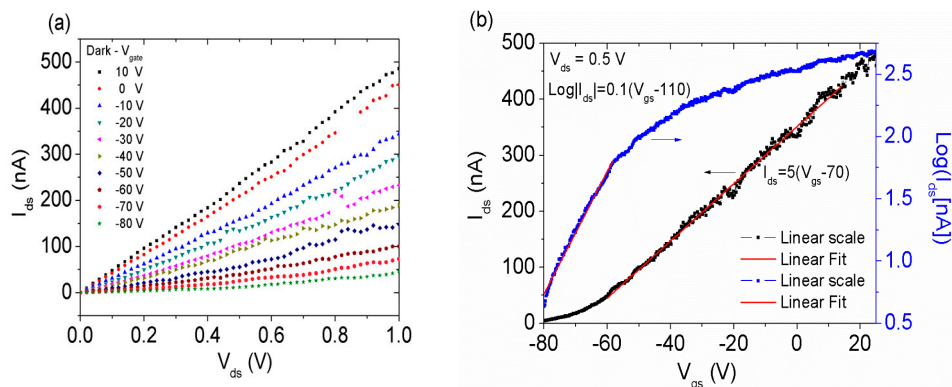
Figure 2. (**a**) Output characteristics $I_{ds} - V_{ds}$ of the MoS_2 transistor for different values of the gate bias V_{gs}; (**b**) Transfer characteristic $I_{ds} - V_{gs}$ (left scale) and $Log|I_{ds}| - V_{gs}$ (right scale) with linear fittings.

We also evaluate the field-effect mobility from the slope of the transfer characteristic (black curve) via the following formula:

$$\mu = \frac{dI_{ds}}{dV_{gs}} \frac{L}{W \cdot C_{ox} \cdot V_{ds}} \tag{1}$$

where $C_{ox} = \varepsilon_{ox}/d_{ox}$ is the oxide capacitance; and ε_{ox} and d_{ox} are the SiO_2 permittivity and thickness, respectively. For 300 nm SiO_2, $C_{ox} = 11$ nFcm^{-2} [45]. The obtained mobility, 0.046 cm^{2}V^{-1}s^{-1}, is on the low side of the range typically reported for uncovered MoS_2—0.05 cm^{2}V^{-1}s^{-1} to 100 cm^{2}V^{-1}s^{-1} [8,33,46,47]. Our value for the field-effect mobility could be slightly underestimated because it does not exclude the effect of the contact resistances [48], which increase the total resistance of the sample and the probability of electron scattering. The low mobility is caused by the mentioned process residues, the long exposure to air, and the likely presence of defects in crystal structure.

3.2. Field Emission Measurements

FE experimentation on a selected flake, shown in Figure 3a, was performed inside the SEM chamber by placing one of the two available W-tips on the metal electrode contacting the flake (cathode) and positioning the other tip (anode) at a variable distance d from the flake, as displayed in Figure 3b.
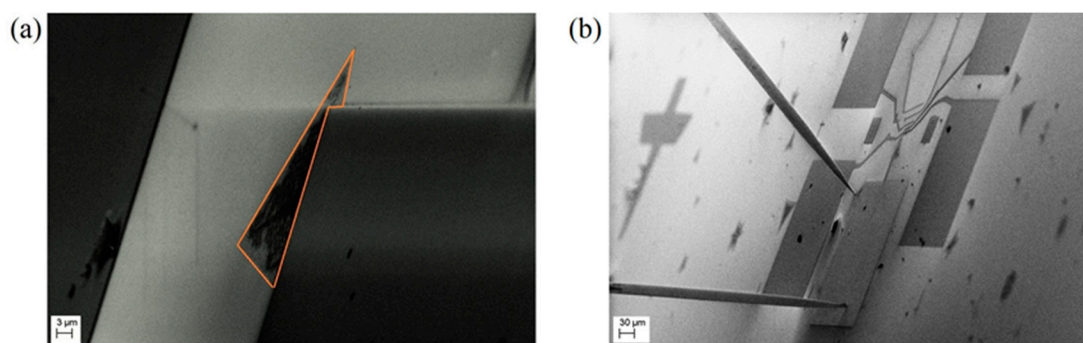
Figure 3. (**a**) SEM image of a MoS_2 flake used for field emission measurements; (**b**) SEM image showing the positioning of the tungsten tips: the lower W-tip is on the metal pad contacting the flake, the other one is placed in front of the flake at a close distance d.

Considering that the MoS_2 flake is n-doped and that the sharp edge originates a high electric field amplification, we expect easy extraction of electrons from the edge of the flake upon application of a voltage. Nevertheless, exposure to air, flake oxidation, and the higher concentration of process residues at the edge make it harder to extract electrons from the flake boundary. On the other hand, due to a better surface quality (less contaminants) in the inner flat part of the flake, and taking advantage of the fine positioning control of our W-tip, we performed field emission characterization supported by SEM imaging from an internal, flat portion of the flake. FE from the flat part of MoS_2 bilayers has not yet been reported in literature and constitutes an interesting way to complete the ongoing investigation of the field emission properties of MoS_2. Similarly, FE measurements on graphene initially gave indication that emitting current was achievable only from edges [49], but it was later demonstrated that FE currents could be extracted from the inner flat part of a graphene flake under application of an electric field of a few hundred V/μm [50].

In Figure 4a,b, we show $I - V$ curves in semilogarithmic and linear scale, respectively, at different anode–cathode distances (i.e., at variable separation between the W-tip and MoS_2 surface). The curves show the typical fluctuations of emission current, indicating desorption of physisorbed molecules caused by Joule heating. Figure 4a shows that reducing the inter-electrode distance causes the field emission current to appear at lower voltages, confirming that the FE turn-on voltage depends on the electrode separation.

For a given distance, the current remains at the floor noise up to a threshold voltage, corresponding to what we define as the FE turn-on voltage; above this threshold it starts rising exponentially up to 100 nA, as expected from Fowler–Nordheim (FN) theory. According to FN model,

$$I = \frac{S a \beta^2 E^2}{\Phi} \exp\left[-\frac{b \Phi^{\frac{3}{2}}}{\beta E} \right] \tag{2}$$

where a and b are constants with values 1.54×10^{-6} A eV V^{-2} and 6.83×10^7 eV$^{\frac{3}{2}}$ V cm^{-1}, respectively; S and ϕ represent the emitting surface and the material work function (in our case $\phi = 5.25$ eV [51]); and β is the so-called field enhancement factor. β is a typical figure of merit for the qualification of field emitting materials, despite the fact that it has been shown to depend on the experimental setup [24]. Finally, the electric field is $E = V/d$, where V is the anode–cathode voltage.

The Fowler–Nordheim behavior of the field emission current is usually checked by the linearity of the so-called FN plot of $\ln\left(I/V^2 \right)$ vs. $1/V$. In particular, the intercept and slope of the fitting straight line yield the emission area and the field enhancement factor β, respectively.

The FN plot of our measurements is reported in Figure 4c, which confirms the expected linear behavior. Figure 4d is analogous to the FN plot for a modified Fowler–Nordheim model recently proposed by Yee Sin Ang et al. [42] to account for 2D electron confinement. This 2D FN model takes into account the fact that, differently from bulk materials, field emission from 2D materials may depend on the extraction direction, resulting in the following current field equation:

$$I_{FN}^{2D} = A_{FN}^{2D} \exp\left[-\frac{b \Phi^{\frac{3}{2}}}{\beta E} \right] \tag{3}$$

where A_{FN}^{2D} is a constant, and the other symbols are the same as in Equation (2). Figure 4c,d show that both models well reproduce the experimental data. However, the 2D model provides a better fit over a wider voltage range. Thus, we use the 2D FN model for further analysis—in particular, to evaluate β at different distances d. The plot in Figure 5a shows linear behavior of $\beta(d)$ in agreement with what has often been reported for different field emission sources [23,33,52,53]. Such behavior is likely due the fact that at higher distance the field from the W-tip becomes more uniform on the emitting area [21].
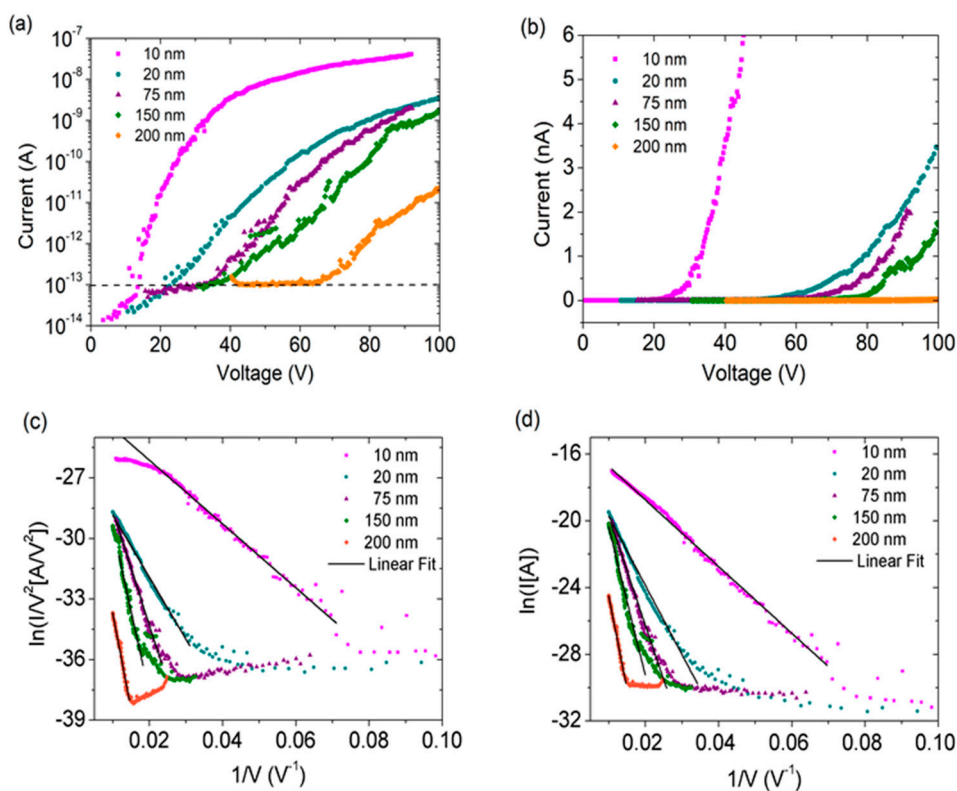
Figure 4. (**a**) Field emission current plotted as a function of applied voltage in semilogarithmic scale; the black line identifies the current level at which the turn-on field is defined; (**b**) Field emission current plotted as a function of applied voltage in linear scale; (**c**) Experimental data plotted with 3D Fowler–Nordheim model; (**d**) Experimental data plotted with modified 2D Fowler–Nordheim model, showing good fit over a wider range.
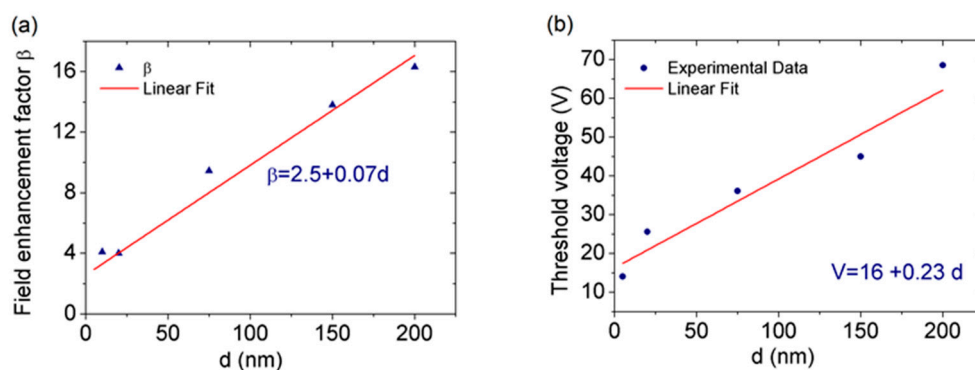
Figure 5. (**a**) Field enhancement factor as a function of the cathode–anode distance; (**b**) Threshold voltage as a function of cathode–anode distance.

The seemingly low value of the amplification factor—less than 20 for d < 200 nm—is remarkable if we consider that emission happens from the inner part of the flake, where no field enhancement by edge effect takes place, and that β further increases with the distance d.

Finally, we can evaluate the turn-on field from the voltage values at which the current emerges from the noise floor of 1×10^{-13} A. From the slope of the fitting straight line of the threshold voltage versus d plot, shown in Figure 5b, we estimate the turn-on field as 230 V/μm. If compared to the typical turn-on field of several kV/μm needed to extract electrons from flat surfaces, the obtained turn-on field can be considered a good result, pointing to noteworthy, although still unexploited, FE capabilities of MoS_2. Like graphene, MoS_2 is a flexible material [54]. The application of an electric

field can cause local warpage of the flake and facilitate FE. Furthermore, surface roughness of the MoS_2 flakes, which strongly depends on the substrate [55], creates wrinkles and protrusions which are favorable to FE. However, the main reason for the lower turn-on field is the n-doping and the low electron affinity of MoS_2, which ranges from 3.74 eV to 4.45 eV [56–58] and is lower than that of graphene.

4. Conclusions

We have presented the electrical transport characterization of field-effect transistors with MoS_2 bilayer channels. The conductance shows an n-type behavior and gate modulation, with prevailing on-state over a wide voltage range. This feature has suggested the use of MoS_2 flakes for field emission investigations. We have reported significant field emission from the flat part of the flake under the application of a moderate electric field, even without taking advantage of field enhancement due to edge effects. We have also demonstrated that a modified field emission model, which considers the 2D nature of the flakes, provides a better fit compared with traditional 3D Fowler–Nordheim theory. This study, demonstrating the suitability of MoS_2 as a field emitter, is a step ahead towards the exploitation of MoS_2 for vacuum electronics applications, in addition to its established use as an electrode in heterojunctions and channel in field-effect transistors.

Author Contributions: A.D.B., F.G. and M.P. conceived and designed the experiments; F.G., M.P. and L.I. performed the experiments; F.U., L.I. and A.D.B. analyzed the data; A.D.B., F.G. and M.P. contributed reagents/materials/analysis tools; F.U. and A.D.B. wrote the paper.

Conflicts of Interest: The authors declare no conflict of interest.

References

1. Schwierz, F. Graphene transistors. *Nat. Nanotechnol.* **2010**, *5*, 487–496. [CrossRef] [PubMed]
2. Avouris, P. Graphene: Electronic and Photonic Properties and Devices. *Nano Lett.* **2010**, *10*, 4285–4294. [CrossRef] [PubMed]
3. Di Bartolomeo, A.; Giubileo, F.; Iemmo, L.; Romeo, F.; Santandrea, S.; Gambardella, U. Transfer characteristics and contact resistance in Ni- and Ti-contacted graphene-based field-effect transistors. *J. Phys. Condens. Matter* **2013**, *25*, 155303. [CrossRef] [PubMed]
4. Di Bartolomeo, A.; Giubileo, F.; Romeo, F.; Sabatino, P.; Carapella, G.; Iemmo, L.; Schroeder, T.; Lupina, G. Graphene field effect transistors with niobium contacts and asymmetric transfer characteristics. *Nanotechnology* **2015**, *26*, 475202. [CrossRef] [PubMed]
5. Zhou, Z.; Yap, Y.K. Two-Dimensional Electronics and Optoelectronics: Present and Future. *Electronics* **2017**, *6*, 53. [CrossRef]
6. Lin, Z.; McCreary, A.; Briggs, N.; Subramanian, S.; Zhang, K.; Sun, Y.; Li, X.; Borys, N.J.; Yuan, H.; Fullerton-Shirey, S.K.; et al. 2D materials advances: From large scale synthesis and controlled heterostructures to improved characterization techniques, defects and applications. *2D Mater.* **2016**, *3*, 042001. [CrossRef]
7. Di Bartolomeo, A.; Genovese, L.; Giubileo, F.; Iemmo, L.; Luongo, G.; Foller, T.; Schleberger, M. Hysteresis in the transfer characteristics of MoS_2 transistors. *2D Mater.* **2018**, *5*, 015014. [CrossRef]
8. Yoon, Y.; Ganapathi, K.; Salahuddin, S. How Good Can Monolayer MoS_2 Transistors Be? *Nano Lett.* **2011**, *11*, 3768–3773. [CrossRef] [PubMed]
9. Late, D.J.; Shaikh, P.A.; Khare, R.; Kashid, R.V.; Chaudhary, M.; More, M.A.; Ogale, S.B. Pulsed Laser-Deposited MoS_2 Thin Films on W and Si: Field Emission and Photoresponse Studies. *ACS Appl. Mater. Interfaces* **2014**, *6*, 15881–15888. [CrossRef] [PubMed]
10. Lopez-Sanchez, O.; Lembke, D.; Kayci, M.; Radenovic, A.; Kis, A. Ultrasensitive photodetectors based on monolayer MoS_2. *Nat. Nanotechnol.* **2013**, *8*, 497. [CrossRef] [PubMed]
11. Feng, Y.; Zhang, K.; Wang, F.; Liu, Z.; Fang, M.; Cao, R.; Miao, Y.; Yang, Z.; Mi, W.; Han, Y.; et al. Synthesis of Large-Area Highly Crystalline Monolayer Molybdenum Disulfide with Tunable Grain Size in a H2 Atmosphere. *ACS Appl. Mater. Interfaces* **2015**, *7*, 22587–22593. [CrossRef] [PubMed]

12. Mak, K.F.; Lee, C.; Hone, J.; Shan, J.; Heinz, T.F. Atomically Thin MoS$_2$: A New Direct-Gap Semiconductor. *Phys. Rev. Lett.* **2010**, *105*, 136805. [CrossRef] [PubMed]

13. Zhou, C.; Wang, X.; Raju, S.; Lin, Z.; Villaroman, D.; Huang, B.; Chan, H.L.-W.; Chan, M.; Chai, Y. Low voltage and high ON/OFF ratio field-effect transistors based on CVD MoS$_2$ and ultra high-k gate dielectric PZT. *Nanoscale* **2015**, *7*, 8695–8700. [CrossRef] [PubMed]

14. Nourbakhsh, A.; Zubair, A.; Joglekar, S.; Dresselhaus, M.; Palacios, T. Subthreshold swing improvement in MoS$_2$ transistors by the negative-capacitance effect in a ferroelectric Al-doped-HfO$_2$/HfO$_2$ gate dielectric stack. *Nanoscale* **2017**, *9*, 6122–6127. [CrossRef] [PubMed]

15. Radisavljevic, B.; Radenovic, A.; Brivio, J.; Giacometti, V.; Kis, A. Single-layer MoS$_2$ transistors. *Nat. Nanotechnol.* **2011**, *6*, 147–150. [CrossRef] [PubMed]

16. Di Bartolomeo, A.; Genovese, L.; Foller, T.; Giubileo, F.; Luongo, G.; Croin, L.; Liang, S.-J.; Ang, L.K.; Schleberger, M. Electrical transport and persistent photoconductivity in monolayer MoS$_2$ phototransistors. *Nanotechnology* **2017**, *28*, 214002. [CrossRef] [PubMed]

17. Zibouche, N.; Kuc, A.; Musfeldt, J.; Heine, T. Transition-metal dichalcogenides for spintronic applications. *Annalen der Physik* **2014**, *526*, 395–401. [CrossRef]

18. Han, W. Perspectives for spintronics in 2D materials. *APL Mater.* **2016**, *4*, 032401. [CrossRef]

19. Lembke, D.; Allain, A.; Kis, A. Thickness-dependent mobility in two-dimensional MoS$_2$ transistors. *Nanoscale* **2015**, *7*, 6255–6260. [CrossRef] [PubMed]

20. Zhong, H.; Quhe, R.; Wang, Y.; Ni, Z.; Ye, M.; Song, Z.; Pan, Y.; Yang, J.; Yang, L.; Lei, M.; et al. Interfacial Properties of Monolayer and Bilayer MoS$_2$ Contacts with Metals: Beyond the Energy Band Calculations. *Sci. Rep.* **2016**, *6*, 21786. [CrossRef] [PubMed]

21. Fowler, R.H.; Nordheim, L. Electron emission in intense electric fields. *Proc. R. Soc. Lond. A* **1928**, *119*, 173–181. [CrossRef]

22. Spindt, C.A.; Holland, C.E.; Rosengreen, A.; Brodie, I. Field-emitter arrays for vacuum microelectronics. *IEEE Trans. Electron Dev.* **1991**, *38*, 2355–2363. [CrossRef]

23. Di Bartolomeo, A.; Scarfato, A.; Giubileo, F.; Bobba, F.; Biasiucci, M.; Cucolo, A.M.; Santucci, S.; Passacantando, M. A local field emission study of partially aligned carbon-nanotubes by atomic force microscope probe. *Carbon* **2007**, *45*, 2957–2971. [CrossRef]

24. Di Bartolomeo, A.; Passacantando, M.; Niu, G.; Schlykow, V.; Lupina, G.; Giubileo, F.; Schroeder, T. Observation of field emission from GeSn nanoparticles epitaxially grown on silicon nanopillar arrays. *Nanotechnology* **2016**, *27*, 485707. [CrossRef] [PubMed]

25. Iemmo, L.; Di Bartolomeo, A.; Giubileo, F.; Luongo, G.; Passacantando, M.; Niu, G.; Hatami, F.; Skibitzki, O.; Schroeder, T. Graphene enhanced field emission from InP nanocrystals. *Nanotechnology* **2017**, *28*, 495705. [CrossRef] [PubMed]

26. Joag, D.S.; More, M.A.; Sheini, F.J. Field Emission from Nanowires. In *Nanowires—Implementations and Applications*; Hashim, A., Ed.; InTech: Rijeka, Croatia, 2011.

27. Lin, P.-H.; Sie, C.-L.; Chen, C.-A.; Chang, H.-C.; Shih, Y.-T.; Chang, H.-Y.; Su, W.-J.; Lee, K.-Y. Field Emission Characteristics of the Structure of Vertically Aligned Carbon Nanotube Bundles. *Nanoscale Res. Lett.* **2015**, *10*, 297. [CrossRef] [PubMed]

28. Giubileo, F.; Di Bartolomeo, A.; Scarfato, A.; Iemmo, L.; Bobba, F.; Passacantando, M.; Santucci, S.; Cucolo, A.M. Local probing of the field emission stability of vertically aligned multi-walled carbon nanotubes. *Carbon* **2009**, *47*, 1074–1080. [CrossRef]

29. Di, Y.; Xiao, M.; Zhang, X.; Wang, Q.; Li, C.; Lei, W.; Cui, Y. Large and stable emission current from synthesized carbon nanotube/fiber network. *J. Appl. Phys.* **2014**, *115*, 064305. [CrossRef]

30. Giubileo, F.; Iemmo, L.; Luongo, G.; Martucciello, N.; Raimondo, M.; Guadagno, L.; Passacantando, M.; Lafdi, K.; Di Bartolomeo, A. Transport and field emission properties of buckypapers obtained from aligned carbon nanotubes. *J. Mater. Sci.* **2017**, *52*, 6459–6468. [CrossRef]

31. Di Bartolomeo, A.; Giubileo, F.; Iemmo, L.; Romeo, F.; Russo, S.; Unal, S.; Passacantando, M.; Grossi, V.; Cucolo, A.M. Leakage and field emission in side-gate graphene field effect transistors. *Appl. Phys. Lett.* **2016**, *109*, 023510. [CrossRef]

32. Suryawanshi, S.R.; More, M.A.; Late, D.J. Exfoliated 2D black phosphorus nanosheets: Field emission studies. *J. Vac. Sci. Technol. B Nanotechnol. Microelectron. Mater. Process. Meas. Phenom.* **2016**, *34*, 041803. [CrossRef]

33. Giubileo, F.; Di Bartolomeo, A.; Iemmo, L.; Luongo, G.; Passacantando, M.; Koivusalo, E.; Hakkarainen, T.V.; Guina, M. Field Emission from Self-Catalyzed GaAs Nanowires. *Nanomaterials* **2017**, *7*. [CrossRef] [PubMed]

34. Choi, W.B.; Chung, D.S.; Kang, J.H.; Kim, H.Y.; Jin, Y.W.; Han, I.T.; Lee, Y.H.; Jung, J.E.; Lee, N.S.; Park, G.S.; et al. Fully sealed, high-brightness carbon-nanotube field-emission display. *Appl. Phys. Lett.* **1999**, *75*, 3129–3131. [CrossRef]

35. Yabushita, R.; Hata, K.; Sato, H.; Saito, Y. Development of compact field emission scanning electron microscope equipped with multiwalled carbon nanotube bundle cathode. *J. Vac. Sci. Technol. B Nanotechnol. Microelectron. Nanometer Struct. Process. Meas. Phenom.* **2007**, *25*, 640–642. [CrossRef]

36. Cole, M.T.; Parmee, R.J.; Milne, W.I. Nanomaterial-based x-ray sources. *Nanotechnology* **2016**, *27*, 1–9. [CrossRef] [PubMed]

37. Gupta, A.P.; Park, S.; Yeo, S.J.; Jung, J.; Cho, C.; Paik, S.H.; Park, H.; Cho, Y.C.; Kim, S.H.; Shin, J.H.; et al. Direct Synthesis of Carbon Nanotube Field Emitters on Metal Substrate for Open-Type X-ray Source in Medical Imaging. *Materials* **2017**, *10*, 878. [CrossRef] [PubMed]

38. Kong, D.; Wang, H.; Cha, J.J.; Pasta, M.; Koski, K.J.; Yao, J.; Cui, Y. Synthesis of MoS_2 and $MoSe_2$ Films with Vertically Aligned Layers. *Nano Lett.* **2013**, *13*, 1341–1347. [CrossRef] [PubMed]

39. Gaur, A.P.S.; Sahoo, S.; Mendoza, F.; Rivera, A.M.; Kumar, M.; Dash, S.P.; Morell, G.; Katiyar, R.S. Cold cathode emission studies on topographically modified few layer and single layer MoS_2 films. *Appl. Phys. Lett.* **2016**, *108*, 043103. [CrossRef]

40. Kashid, R.V.; Late, D.J.; Chou, S.S.; Huang, Y.-K.; De, M.; Joag, D.S.; More, M.A.; Dravid, V.P. Enhanced Field-Emission Behavior of Layered MoS_2 Sheets. *Small* **2013**, *9*, 2730–2734. [CrossRef] [PubMed]

41. Li, Y.B.; Bando, Y.; Golberg, D. MoS_2 nanoflowers and their field-emission properties. *Appl. Phys. Lett.* **2003**, *82*, 1962–1964. [CrossRef]

42. Sin Ang, Y.; Zubair, M.; Ooi, K.J.A.; Ang, L.K. Generalized Fowler-Nordheim field-induced vertical electron emission model for two-dimensional materials. *arXiv*, 2017.

43. Li, X.; Zhu, H. Two-dimensional MoS2: Properties, preparation, and applications. *J. Materiomics* **2015**, *1*, 33–44. [CrossRef]

44. Guo, Y.; Robertson, J. Origin of the high work function and high conductivity of MoO_3. *Appl. Phys. Lett.* **2014**, *105*, 222110. [CrossRef]

45. Jariwala, D.; Sangwan, V.K.; Late, D.J.; Johns, J.E.; Dravid, V.P.; Marks, T.J.; Lauhon, L.J.; Hersam, M.C. Band-like transport in high mobility unencapsulated single-layer MoS_2 transistors. *Appl. Phys. Lett.* **2013**, *102*, 173107. [CrossRef]

46. Radisavljevic, B.; Kis, A. Mobility engineering and a metal–insulator transition in monolayer MoS_2. *Nat. Mater.* **2013**, *12*, 815. [CrossRef] [PubMed]

47. Amani, M.; Chin, M.L.; Birdwell, A.G.; O'Regan, T.P.; Najmaei, S.; Liu, Z.; Ajayan, P.M.; Lou, J.; Dubey, M. Electrical performance of monolayer MoS_2 field-effect transistors prepared by chemical vapor deposition. *Appl. Phys. Lett.* **2013**, *102*, 193107. [CrossRef]

48. Giubileo, F.; Di Bartolomeo, A. The role of contact resistance in graphene field-effect devices. *Prog. Surf. Sci.* **2017**, *92*, 143–175. [CrossRef]

49. Xiao, Z.; She, J.; Deng, S.; Tang, Z.; Li, Z.; Lu, J.; Xu, N. Field Electron Emission Characteristics and Physical Mechanism of Individual Single-Layer Graphene. *ACS Nano* **2010**, *4*, 6332–6336. [CrossRef] [PubMed]

50. Santandrea, S.; Giubileo, F.; Grossi, V.; Santucci, S.; Passacantando, M.; Schroeder, T.; Lupina, G.; Di Bartolomeo, A. Field emission from single and few-layer graphene flakes. *Appl. Phys. Lett.* **2011**, *98*, 163109. [CrossRef]

51. Choi, S.; Shaolin, Z.; Yang, W. Layer-number-dependent work function of MoS_2 nanoflakes. *J. Korean Phys. Soc.* **2014**, *64*, 1550–1555. [CrossRef]

52. Passacantando, M.; Bussolotti, F.; Santucci, S.; Di Bartolomeo, A.; Giubileo, F.; Iemmo, L.; Cucolo, A.M. Field emission from a selected multiwall carbon nanotube. *Nanotechnology* **2008**, *19*, 395701. [CrossRef] [PubMed]

53. Xu, X.; Zhai, T.; Shao, M.; Huang, J. Anodic formation of anatase TiO_2 nanotubes with rod-formed walls for photocatalysis and field emitters. *Phys. Chem. Chem. Phys.* **2012**, *14*, 16371–16376. [CrossRef] [PubMed]

54. Bertolazzi, S.; Brivio, J.; Kis, A. Stretching and Breaking of Ultrathin MoS_2. *ACS Nano* **2011**, *5*, 9703–9709. [CrossRef] [PubMed]

55. Quereda, J.; Castellanos-Gomez, A.; Agraït, N.; Rubio-Bollinger, G. Single-layer MoS$_2$ roughness and sliding friction quenching by interaction with atomically flat substrates. *Appl. Phys. Lett.* **2014**, *105*, 053111. [CrossRef]

56. Sup Choi, M.; Lee, G.-H.; Yu, Y.-J.; Lee, D.-Y.; Hwan Lee, S.; Kim, P.; Hone, J.; Jong Yoo, W. Controlled charge trapping by molybdenum disulphide and graphene in ultrathin heterostructured memory devices. *Nat. Commun.* **2013**, *4*, 1624. [CrossRef] [PubMed]

57. Das, S.; Chen, H.-Y.; Penumatcha, A.V.; Appenzeller, J. High Performance Multilayer MoS$_2$ Transistors with Scandium Contacts. *Nano Lett.* **2013**, *13*, 100–105. [CrossRef] [PubMed]

58. Kang, J.; Tongay, S.; Zhou, J.; Li, J.; Wu, J. Band offsets and heterostructures of two-dimensional semiconductors. *Appl. Phys. Lett.* **2013**, *102*, 012111. [CrossRef]